25th ABCM International Congress of Mechanical Engineering
October 20-25, 2019, Uberlândia, MG, Brazil

COB-2019-1376
INVESTIGATION OF JET-FLAP INTERACTION NOISE THROUGH NUMERICAL SIMULATIONS BASED ON THE LATTICE BOLTZMANN METHOD

Renatto M. Yupa-Villanueva
Gil F. Greco
Graduate Program of Mechanical Engineering (POSMEC), Federal University of Santa Catarina, Florianópolis, SC 88040-900, Brazil.
renatto.villanueva@polo.ufsc.br
gil.greco@lva.ufsc.br

José R. L. N. Sirotto
Graduate Program of Mechanical Engineering (POSMEC), Federal University of Santa Catarina, Florianópolis, SC 88040-900, Brazil.
joserodrigues.neto@lva.ufsc.br

Filipe D. da Silva
Department of Mobility Engineering, Federal University of Santa Catarina, Joinville, SC 89219-600, Brazil.
filipe.dutra@ufsc.br

Cesar J. Deschamps
Department of Mechanical Engineering, Federal University of Santa Catarina, Florianópolis, SC 88040-900, Brazil
deschamps@polo.ufsc.br

Abstract. *One of the main sources of aircraft noise during takeoff condition is caused by the exhaust jet from the engine. Therefore, studies in this area have gained importance with the rise of stricter noise regulations. In this paper, a numerical analysis of a cold single-flow under both isolated and installed configurations were conducted. The flow conditions were, acoustic Mach number* M_a *= 0.7, freestream Mach number* M_∞ *= 0 and jet temperature ratio to the ambient of* T_J/T_∞ *= 0.95. The installed configuration considered a flapped plate with trailing edge (TE) placed at a distance* X/D_J *= 3.20 measured from the nozzle exit and at a radial distance* $H/D_J = 0.59$ *from the jet axis. Experimental tests were performed for polar angles 60°≤θ≤150° with Δθ=10°, where 180° corresponds to the downstream direction of the jet nozzle. Numerical results were obtained using Very Large Eddy Simulations (VLES) based on the Lattice Boltzmann Method (LBM). The numerical far-field noise predictions were obtained through the permeable Ffowcs-Williams Hawkings (FW-H) integral formulation. Grid resolution studies were carried out to assess numerical truncation error. The numerical results were then validated through comparisons with measurements of Sound Pressure Level (SPL) with differences around of 2.5 dB in 1/3 octave bands being observed at θ=90°. Low-frequency noise amplifications were predicted occurring at the unshielded and shielded sides of the installed case, being mainly dominant at the polar angles θ<90°. The installed configuration presented Overall Sound Pressure Levels about 6.5 dB and 9.5 dB higher in comparison to the isolated jet for both shielded and unshielded sides, respectively. Contours of SPL as function of St and polar angles showed higher noise levels in the low St range (St<0.68).*

Keywords: *Jet noise, Jet-flap interaction, Lattice-Boltzmann Method, Aeroacoustics.*

1. INTRODUCTION

It is well-known that the close integration of high bypass ratio engines with the aircraft high lift devices (HLD), such as wing and flaps, generate additional noise sources known as Jet-Installation Noise (JIN). The installation effects are responsible for changing the sound directivity depending on the configuration of the solid surfaces (i.e. HLDs) in respect to the engines exhaust flow (Hoheisel and von Geyr, 2012; Jente *et al.*, 2018). Therefore, the understanding behind the installation noise is crucial to improve the design of the next generations of aircrafts that will come during the following years.

Recent studies addressed jet-flap interaction noise via parametric experimental analysis (Lawrence and Self, 2015;

Jordan *et al.*, 2018; Lee *et al.*, 2019). As the cost involved in these facilities is quite elevated, numerical simulations are a viable and efficient approach as a complement to the experiments in jet noise studies. Moreover, numerical simulations can provide detailed results of the flow and acoustic fields that are not feasible to obtain experimentally.

In this context, many studies on this subject have been addressed numerically. For instance, Semiletov *et al.* (2013); Kopiev *et al.* (2014) and Mockett *et al.* (2017) used Large Eddy Simulation (LES) and hybrid LES-RANS to predict jet wing-flap interaction noise together with the Ffowcs-Williams and Hawkings approach (Mendez *et al.*, 2013) to analyze the far-field noise. The results showed reasonable agreement with experimental data, with deviations of about 3-4 dB relative to the reference data. Lyubimov *et al.* (2014) studied the effect of jet-flap interaction noise experimentally and numerically under static-subsonic conditions. It was found that the excess noise is related to jet deformation and increasing velocity gradients within the jet flow which are induced by flap tip vortex. More recently, Tyacke *et al.* (2019) studied numerically the effect of the flap trailing edge considering a coaxial jet isolated/installed with flight stream. An increase of 20 dB was predicted at upstream polar angles due to the installation effects with flight stream. At similar conditions, Mengle (2011) reported an increase compared with isolated of approximately 10 dB under static conditions, and 15 dB with a flight stream of $M_{\mathrm{J}} = 0.28$.

Another alternative is to use the Lattice-Boltzmann/Very Large Eddy Simulation Method (LBM-VLES) to predict the noise radiation due to the interaction between jet and flap. An extended LBM-VLES for high subsonic jet noise prediction was proposed by Lew *et al.* (2014), with promising results for cold and heated high-speed jet noise prediction for a single-stream nozzle. Da Silva *et al.* (2015) investigated the installation effects caused by the interaction between a cold jet ($M_{\mathrm{J}} = 0.5$ and $M_{\mathrm{J}} = 0.4$) and a flat plate. The computational simulations were capable of capturing the installation effects for different polar angles with good accuracy. However, simulations of high subsonic jet flows remained a challenge due to the presence of compressibility effects. In this sense, a LBM based entropy solver was proposed and validated by van der Velden *et al.* (2018) and used to assess the installation effects on jet noise in coaxial jet flows (Rego *et al.*, 2019).

This paper reports an investigation of the prediction capabilities of the LBM-based code PowerFLOW® (V6.0) for the simulation of single-stream jet under isolated and installed configurations (jet-flapped plate) with reference to measurements for both configurations obtained in an experimental setup.

2. EXPERIMENTAL SETUP

The experiments were carried out at the jet rig facility of the Federal University of Santa Catarina, which is illustrated in Figure 1. This facility was designed and validated to perform tests with single subsonic cold jets (Sirotto *et al.*, 2016; Bastos *et al.*, 2018). The facility is composed of nine main elements: i) compressor, ii) filter, iii) dryer, iv) check valves, v) pressure vessel, vi) control valve, vii) plenum, viii) nozzle and ix) anechoic chamber. The plenum upstream the nozzle is used to filter the noise generated by the air supply system itself and to evaluate the acoustic Mach number of the jet based on the isentropic flow condition. For this investigation, experiments were carried out using a duct of 2 m of length with 2-inch exit diameter of the SMC000 nozzle (Brown and Bridges, 2006). All workbench operations are controlled by an integrated system developed with the LabView software.

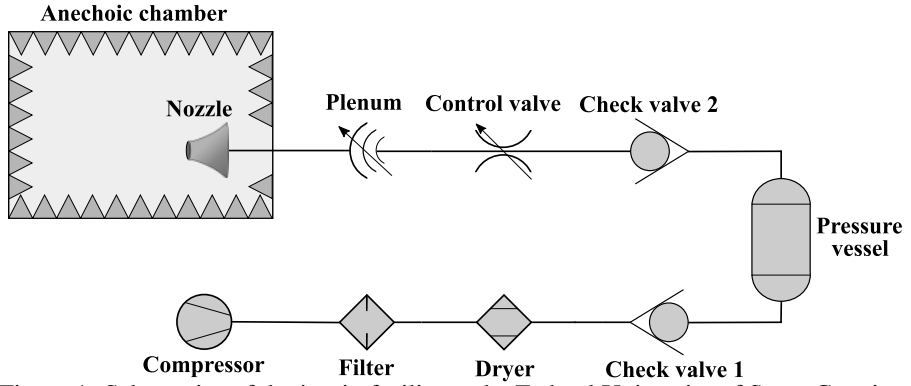

Figure 1: Schematics of the jet rig facility at the Federal University of Santa Catarina.

The flow conditions are characterized by a cold, subsonic jet, with acoustic Mach number M_{a} = 0.7 in static conditions M_{∞} = 0 and jet temperature ratio $T_{\mathrm{J}}/T_{\infty}$ = 0.95 for both isolated and installed configurations. The data acquisition was carried out using a polar array with 10 microphones (1/4" free-field/model G.R.A.S. 46BE-S1) centered on the nozzle exit at a radial distance of 2.10 m ($\sim 41D_{\mathrm{J}}$), which are distributed from 60° to 150° at 10° intervals, as illustrated in Figure 2. The signals were acquired during 30 seconds by a NI PXIe-1082 data acquisition system (DAQ) with a sampling frequency of 120 kHz. The data was collected for a frequency range of 500 Hz to 36 kHz in Δf= 25 Hz narrow bands. Hanning windowings with 50% overlap were applied to minimize energy leakage, leading to 3000 spectral averages along the measured pressure time-histories. The background noise during the measurements was not greater than 35 dB for all microphones. The single convergent nozzle in this work had an inlet diameter of 6-inches (~152.5 mm) followed by a

contraction of 27° and a conical slope of 5° with effective exit diameter of 2-inches (D_J = 50.8 mm), as proposed by Brown and Bridges (2006). The flapped plate is composed of i) flat plate and ii) inclined flat flap (15° measured between the nozzle exit axis and the flat flap longitudinal axis). The span length and the thickness of the flapped plate are $L_\mathrm{s}/D_\mathrm{J}$ = 15 and e/D_J = 0.25, respectively. The chords of the flapped plate are $L_\mathrm{fp}/D_\mathrm{J}$ = 2.38 and $L_\mathrm{iff}/D_\mathrm{J}$ = 0.82 for both flat plate and the inclined flat flap, respectively.

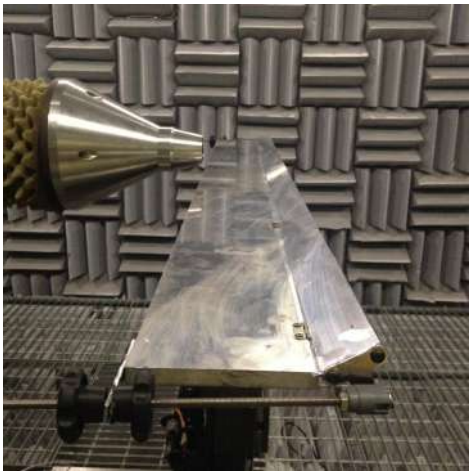

(a) Experimental setup with the flapped plate and the convergent nozzle SMC000.

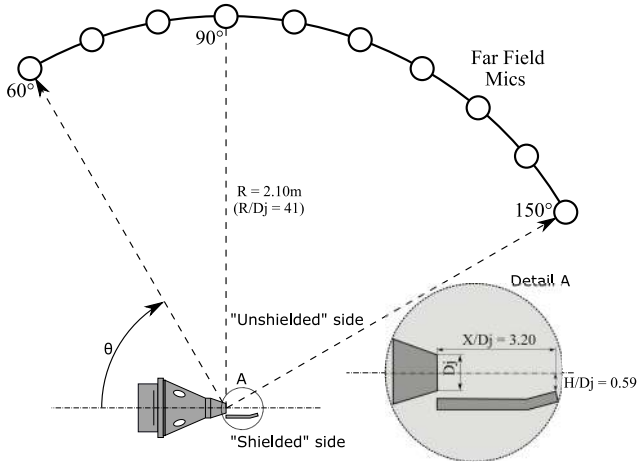

(b) Microphone array around of the jet nozzle for the installed configuration.

Figure 2: Geometrical configurations used in the test facility.

3. COMPUTATIONAL MODEL

3.1 Flow solver

The Boltzmann equation is described by the distribution function f_i(**x**,t,**v**), from which through the Chapman-Enskog expansion (Chapman *et al.*, 1990) it is possible to obtain the Navier-Stokes equations. In addition, macroscopic flow properties (**u**, ρ, T,...) can be recovered by statistical moments of the distribution function. The Lattice Boltzmann Method (LBM) resolve the Boltzmann Equation by discretizing the space velocity domain into a prescribed number of values in magnitude and direction (Guo and Shu, 2013). The LBM-based code Powerflow® (V6.0) uses 19 stencil points through the D3Q19 model. The standard LBM formulation is based on the (dimensionless) time-explicit advection equation:

$$f_i(\mathbf{x} + \mathbf{v}_i\Delta t, t + \Delta t) - f_i(\mathbf{x}, t) = \Omega_i(\mathbf{x}, t), \tag{1}$$

where f_i represents the particle distribution function along the i-th direction, according to the finite set of discrete velocities ($\mathbf{v}_i$: i=0, ..., 18). The terms $\mathbf{v}_i\Delta t$ and Δt are the space and time increments, respectively. The collision operator (Ω_i) represents the rate of change of f_i due to the particle's interaction and is approximated by using the Bhatnagar-Gross-Krook (BGK) collision model (Bhatnagar *et al.*, 1954):

$$\Omega_i(\mathbf{x}, t) = \frac{-\Delta t}{\tau}[f_i(x, t) - {f_i}^{\mathrm{eq}}], \tag{2}$$

where the relaxation time τ is related to the kinetic viscosity, ν, as $\tau = (\nu + 0.5)/T$. The equilibrium function in the code is approximated by a third order polynomial expansion. The w_i represent the weighting factors, 1/18 for 6 coordinate directions, 1/18 for the 12 bi-diagonal directions and 1/3 for the rest particle according to the D3Q19 model and T is the temperature in lattice units

$${f_i}^{\mathrm{eq}} = \rho w_i \left[1 + \frac{\mathbf{v}_i\mathbf{u}}{T} + \frac{(\mathbf{v}_i\mathbf{u})^2}{2T^2} - \frac{(\mathbf{u}^2)}{2T} + \frac{(\mathbf{v}_i\mathbf{u})^3}{6T^3} - \frac{\mathbf{v}_i\mathbf{u}}{2T^2}\mathbf{u}^2\right]. \tag{3}$$

For high Reynolds flows, turbulence modelling is incorporated into the LBM scheme (Chen *et al.*, 2003) by solving a modified two-equation k-ε model based on the original renormalization group (RNG) formulation (Teixeira, 1998). This approach is commonly referred as LBM Very Large Eddy Simulation (LBM-VLES). In this context, the turbulence model is used to evaluate an effective turbulent relaxation time. Since an excessive computational resource would be required to solve the viscous sub-layer for high Reynolds number, the code uses a wall function approach, which is based on the standard law-of-the-wall (Launder and Spalding, 1983). To ensure numerical stability, particularly for Mach numbers greater than 0.5, the code incorporates an LBM based entropy solver to account for flow compressibility effects. The

second distribution function is based on a specific scalar quantity (Chen and Zhang, 2013), ensuring the total conservation by multiplying the second scalar distribution with the fluid particle distribution and employs an extended collision operator based on a unique Galilean invariant form (Chen *et al.*, 2017).

3.2 Far-Field acoustic prediction

In this investigation, the Ffowcs-Williams and Hawkings (FW-H) solver implemented by Brès *et al.* (2010), which is based on a forward-time solution of the formulation 1A extended to a permeable (porous) integration surface (Farassat and Succi, 1982) is used to compute the far-field noise. For this investigation, two different geometries of permeable FW-H surfaces were considered. For the isolated case, a conical shape was employed (Figure 3a). The chosen length was $26D_{\mathrm{J}}$ in order to ensure that the most significant noise sources were fully encompassed by the FW-H surface. For the installed case, the FW-H was enlarged, (Figure 3b) so that the additional noise sources generated by the presence of the flapped plate could also be captured. At the downstream region of the permeable FW-H surfaces, hydrodynamic perturbations are advected through the ending-surface, resulting in spurious hydrodynamic noise sources of sound. For this reason, assuming that these hydrodynamic sources of noise are uncorrelated, it is possible to minimize their spurious effects on the far-field predictions through a time-averaged strategy by using seven (7) closing discs located at the end of each FW-H surface, following the recommendation of Shur *et al.* (2005) and Mendez *et al.* (2013).

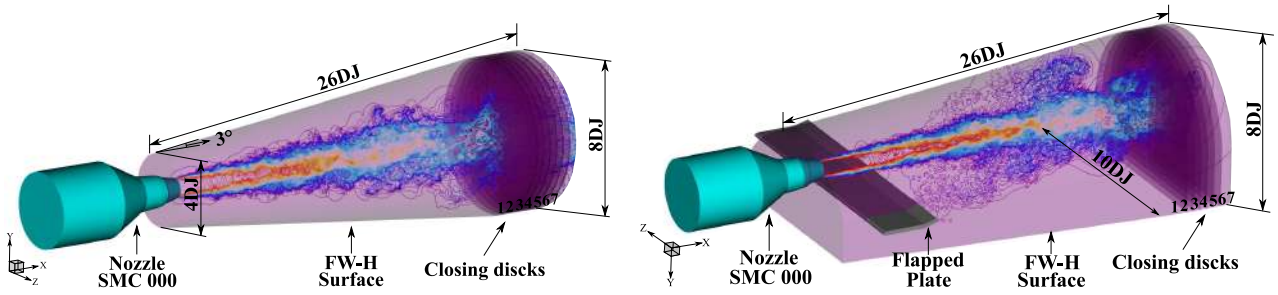

(a) Isolated jet. (b) Installed jet.

Figure 3: Permeable FW-H surfaces used for far-field noise predictions.

The configuration of the permeable FW-H surface is characterized by two parameters: (i) the FW-H spatial grid resolution ($\Delta x_{\mathrm{FW-H}}$), which is based on the smaller wavelengths of interest; (ii) the sampling frequency (f_{s}), which defines the maximum frequency of analysis. Both parameters were chosen considering both computational storage and prediction accuracy. For this investigation, the FW-H spatial grid resolution chosen was $D_{\mathrm{J}}/8$. The sampling frequency was $8f_{\max}$ with $f_{\max}$=36 kHz.

3.3 Simulation setup

The simulation model was prepared to represent the jet configurations of the experiment, which are presented in Figure 2a. Boundary conditions (BC) of total pressure, P_0, and total temperature, T_0, were prescribed at the nozzle inlet, which were obtained from isentropic relations in order to reach the desirable Mach number and temperature ratio at the nozzle exit. A buffer zone, with increased viscosity, is set to prevent the formation of any acoustical field inside the nozzle. An external artifact known as "trip", which assist the computational scheme to trigger flow instabilities, is employed to ensure a fully developed turbulent flow at the nozzle exit by disturbing the nozzle boundary layer at the nozzle inner walls. Regarding the solid surfaces, all the nozzle interior walls adopted the no-slip flow condition, as well as solid walls of the trip and the flapped plate. For this study a freestream Mach number of 1% of the jet velocity at the nozzle exit was imposed to help the jet entrainment, following Brès *et al.* (2012).

The computational domain is composed by fourteen (14) variable resolution regions, where VR 0 and VR 13 are the coarsest and finest grid resolutions, respectively. The VR 0 corresponds to the global domain keeping a cubic shape with 52 m (~1024 D_j) of each side. In order to minimize numerical wave dispersion in the desired frequency range, the FW-H surfaces were positioned totally inside the VR 10 zone, as depicted in Figure 4. The length of the VR 11 was determined using an empirical relationship proposed by Witze (1974) to adequately discretize the potential core of the jet. The VR 13 contains the finest mesh elements, which is employed to properly discretize flow regions with high shear stress, i.e. next to the nozzle inner walls and in the mixing layer formed after the nozzle exit. The full simulation is composed of two periods: (i) transient time and (ii) acquisition time. The transient time is considered to be (10) times longer the time required by an acoustic wave to travel a distance equal to the streamwise extension of the FW-H surface. The acquisition time is calculated based on the minimum frequency of interest $f_{\min}$ =134 Hz ($\mathrm{St}_{\min}$=0.04), whose inverse is multiplied by a factor $\beta_{\mathrm{s}} = 15$. This factor takes into account the number of desired spectral averages (30) times the window overlap factor (50%).

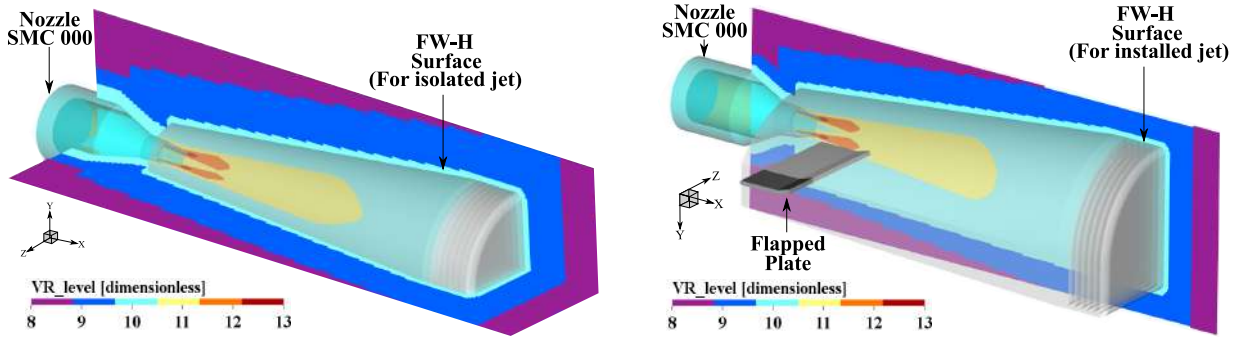

(a) Isolated jet. (b) Installed jet.

Figure 4: Details of the simulation setup: VR configuration and permeable FW-H surfaces.

4. VALIDATION ANALYSIS

A mesh convergence study was performed to assess the sensitivity of the numerical far-field acoustic predictions to both the isolated and installed configurations. In order to reduce the total simulation time, the results obtained with coarser meshes were used as initial condition for simulations with finer meshes. Required computational resources are provided in Table 1, where the global mesh resolution is defined as the nozzle exit diameter divided by the finest element to characterize each resolution level. In addition, the number of voxels is presented for each resolution level, with the installed case having higher density of voxels as result of the FW-H shape and the presence of the flapped plate. The fine mesh required 18.7 kCPUh and 20.1 kCPUh, distributed over 480 cores for the isolated jet and installed jet, respectively. The validation of the computational model was carried out through comparisons between predictions and measurements of far-field noise, as will be shown in Sections 4.1 and 4.2.

Table 1: Grid matrix information and computational cost for both isolated and installed configurations.

Case	Resolution level	Resolution	Voxel size at nozzle exit [mm]	Number of Voxels [10^6]	kCPUh
Isolated	Coarse	256	0.198	102.7	2.7
	Medium	360	0.141	228.4	5.4
	Fine	512	0.099	563.4	18.7
Installed	Coarse	256	0.198	127.9	3.4
	Medium	360	0.141	298.1	6.8
	Fine	512	0.099	766.0	20.1

4.1 Far-field spectra

The effect of the mesh resolution in the far-field spectra is analyzed in terms of 1/3 octave bands Sound Pressure Level (SPL), considering a reference pressure of 20 μPa, for $\theta = 90°$ for both isolated and installed configurations (see Figure 5). The frequency is expressed in dimensionless form via the Strouhal number, defined as $\mathrm{St} = fD_\mathrm{J}/U_\mathrm{J}$, where U_J is the mean axial velocity at the jet exit.

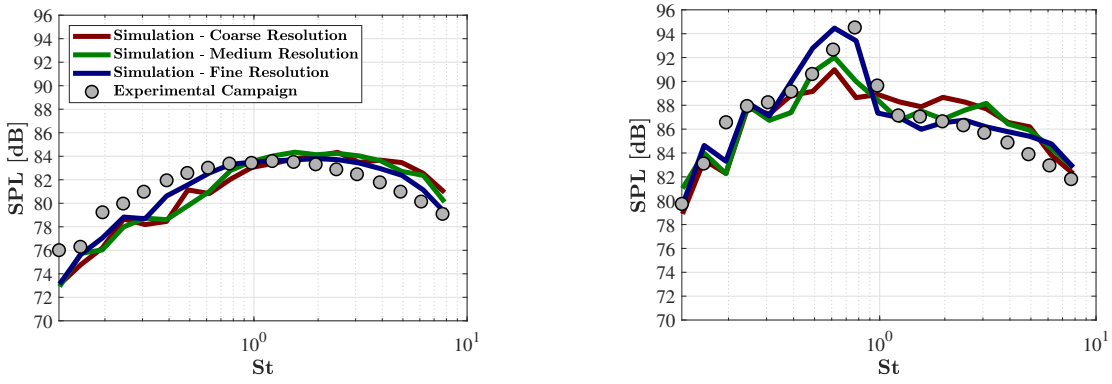

(a) Isolated jet. (b) Installed jet.

Figure 5: Grid convergence analysis for both isolated and installed configurations expressed in Sound Pressure Level (SPL) 1/3 octave bands for θ=90°.

From the curves of Figure 5a, the spectral shape of the isolated jet for the three resolution levels were reasonably predicted by the simulations. At St<0.85, the predicted noise levels tend to increase as the mesh is refined, while for St>1.2 the SPL predictions present an opposite behavior. By considering the finest mesh, underpredictions for St<0.85 and overpredictions for St>1.2 can be observed in Figure 5a. Maximum deviations between the numerical results and the experimental data around of 2.3 dB at St=0.3 and 1.5 dB at St=4.87 were predicted.

As well as for the isolated jet, the spectral shape of the installed jet was reasonably predicted by considering the three resolution levels as observed in Figure 5b. For St<0.3, the SPL predictions had very similar noise levels with a slight difference up to 1 dB at St=0.19 between the fine mesh and the other mesh resolutions. For St range 0.3<St<0.97, the finest mesh presented better predictions than the coarse and medium meshes. At this St range, the increase of noise was better predicted with mesh refinements. For St>0.97, the coarse and medium meshes presented higher noise levels in comparison with the fine mesh. By comparing the fine mesh with experimental data, the numerical results presented underpredictions at St<0.3, overpredictions at 0.3<St<0.65, underpredictions at 0.65<St<2.0 and overpredictions at St>2.0 with maximum deviations around of 2.5 dB, 2.1 dB, 2.2 dB and 1.8 dB at each St range, respectively. Although the numerical results present a clear shift in relation to the experimental data, the trends were well predicted.

4.2 OASPL Polar directivity

The Overall Sound Pressure Level (OASPL) was calculated for a frequency range from 500 Hz to 36 kHz (0.1<St<8.0) with Δf= 100 Hz for polar angles 60°$\leq\theta\leq$150° with $\Delta\theta$=10°. Good agreement was observed between numerical predictions and experimental data for the isolated jet, as shown in Figure 6a, with differences of less than 1 dB occurred regardless the mesh resolution. For the installed case (Figure 6b), noise levels were underpredicted up to 1 dB for the coarse mesh and 0.5 dB for the medium mesh for the considered angles. By contrast, the simulation with the fine mesh slightly underpredicted, overpredicted and underpredicted the noise for θ=60°, 70°$\leq\theta\leq$100° and 110°$\leq\theta\leq$150°, respectively. A better trend is observed for the considered angles, as the mesh resolution is increased. The higher deviations occur for 60°$\leq\theta\leq$100° with less than 0.25 dB for the fine mesh. The installation effects in terms of relative Overall Sound Pressure Levels (ΔOASPL) is presented in Figure 6c. Good agreement with experimental data was achieved with medium and fine meshes. Maximum relative deviations were about 0.6 dB at θ=70° and θ=140° with the fine mesh. The installation effects achieved a maximum value of 7.0 dB at θ=60° for the considered angles, revealing that the noise is very sensitive to the presence of the flapped plate.

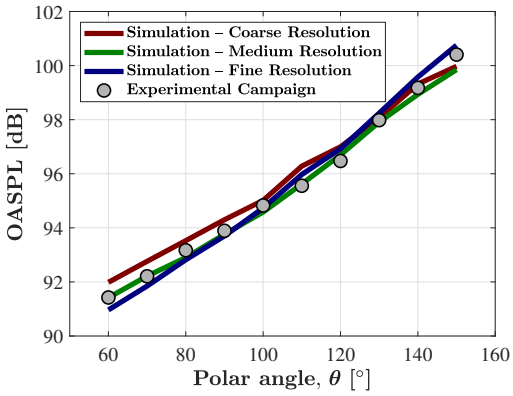

(a) Isolated jet.

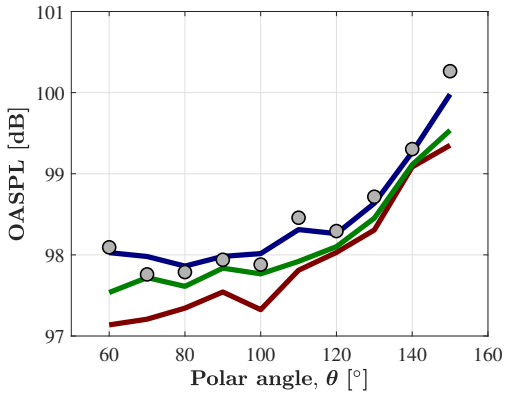

(b) Installed jet.

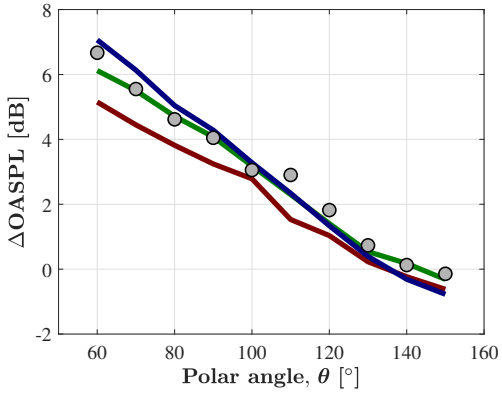

(c) ΔOASPL (Installation effects).

Figure 6: OASPL computed for St range 0.1<St<8.0 at the unshielded side for 60°$\leq\theta\leq$150°.

The deviations observed between predictions and measurements can be in part due to differences between the numerical model and the experimental setup, i.e., chamber size, nozzle duct length and nozzle acoustic treatment. Moreover, the results presented herein should also be analyzed with caution due to the fact that the mesh convergence was not totally achieved. Nevertheless, the trends predicted by the numerical model for the far-field noise at different polar angles are consistent with the experimental data.

5. JET – FLAPPED PLATE NOISE ANALYSIS

5.1 Installation Effect

The polar directivity for both isolated and installed jets are shown through the absolute and relative OASPL in Figure 7. The OASPL was calculated for the same frequency range considered in Section 4.2 when using the fine mesh. The directivity pattern observed for the isolated jet is in agreement with the studies presented by MacGregor *et al.* (1973), caused by effects of convection and sound refraction. By comparing the installed case with the isolated case, higher noise levels occur for all polar angles lower than 130° in the unshielded side as shown in Figure 7a. Similar trends can be observed for the shielded side, but in a broader polar range. Head and Fisher (1976) suggested that the most dominant source of interaction noise is generated by the turbulence within the free shear layer of the jet convecting downstream past the trailing edge (TE) of the wing or flap. This additional noise can be explained mainly by two mechanisms: (i) due to unsteady loadings on the flapped plate surface as was predicted by Curle (1955) and (ii) due to the difraction of the jet's hydrodynamic near-field about the TE (Ffowcs-Williams and Hall, 1970). The relative OASPL values between the installed and isolated jets in Figure 7b show the noise is increased by up to 9.5 dB at the unshielded side and by up to 6.9 dB at the shielded side for θ<90°. This result can be associated with the flap deflections as was studied by Nogueira *et al.* (2017, 2019) through an inclined plate.

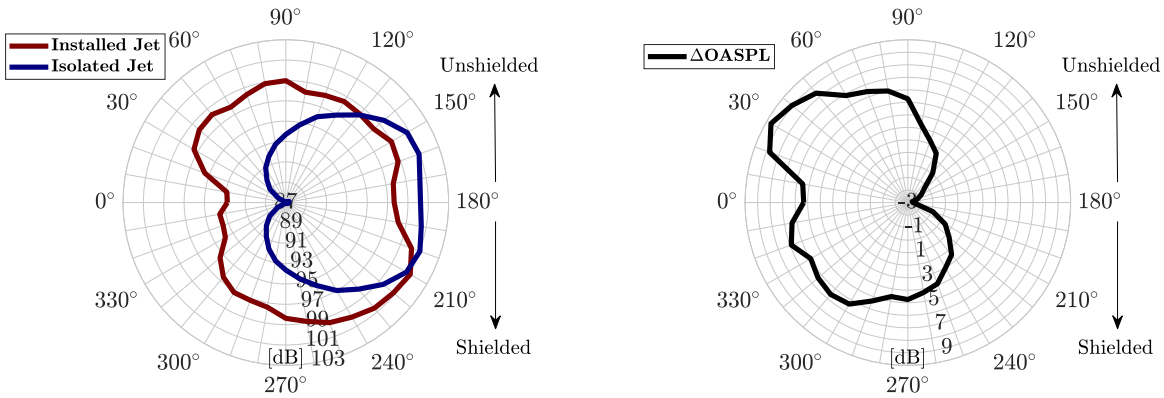

(a) OASPL for isolated and installed jets.

(b) ΔOASPL (installation effects).

Figure 7: OASPL Polar directivities computed for St range 0.1<St<8.0.

5.2 SPL's dependance on St and polar angles

The Contours of SPL as a function of St and polar angles for the isolated and installed jets are presented in Figure 8, as well as the increase of noise due to installation effects quantified by the metric ΔSPL=SPL$_{\mathrm{Inst}}$-SPL$_{\mathrm{jet}}$. Directivity is highly dependent on the Strouhal number for both cases. For the isolated case, high values of far-field noise occur for 150°<θ<210° at 0.1<St<0.34, mainly in St=0.13, as shown in Figure 8a.

Examining Figure 8b, one can observe that the highest noise levels for the installed case occur at St<0.68 with similar levels at both unshielded and shielded sides. At this St range, the noise amplifications observed for θ<160° and θ>200° is likely to occur resulting from trailing edge scattering, as observed by Head and Fisher (1976). For St>0.85, the noise levels are dominated by the jet quadrupoles at both unshielded and shielded sides. In this St range, noise levels for the unshielded side and polar range θ<90° are approximately 3 dB higher in comparison to the same directions of the shielded side.

The Contours of ΔSPL depicted in Figure 8c show that the highest ΔSPL are in the low range of St (0.13<St<0.68), suggesting that the flap portion produces high noise levels. Likewise a directivity pattern could be associated to the inclination angle of the flap. By comparing the noise levels of the unshielded and shielded sides, a slight asymmetry can be observed by the presence of the flapped plate, where one can clearly identify the St range and directivity angles most affected by the presence of the flapped plate. In this case, noise levels can be up to 20 dB higher when compared to the isolated jet for the St range of 0.34<St<0.68 and polar angles of 10°<θ<70°. For St>0.85, the noise levels are approximately 3 dB higher than the isolated case at θ=90° due to reflection effects. For θ=270° and at the same St range, the blockage effect was observed. These effects indicate that sound reflection/blockage are the main installation effects at this St range for both unshielded and shielded sides, respectively, as was also reported by Lawrence (2014).

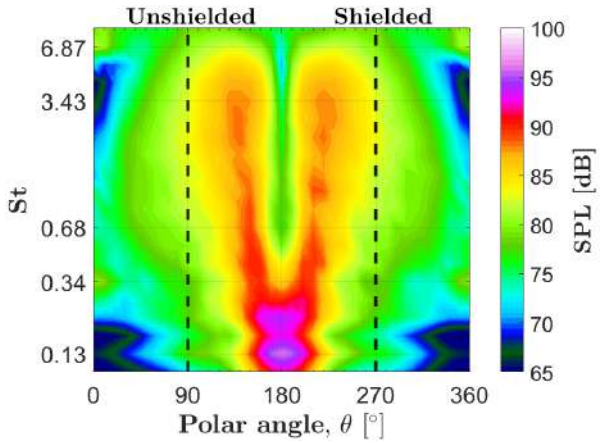

(a) Isolated jet.

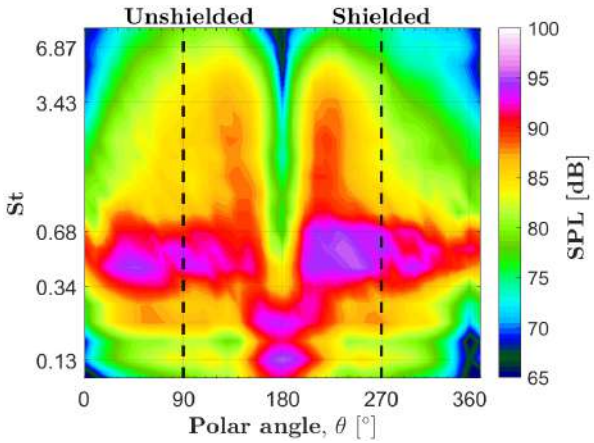

(b) Installed jet.

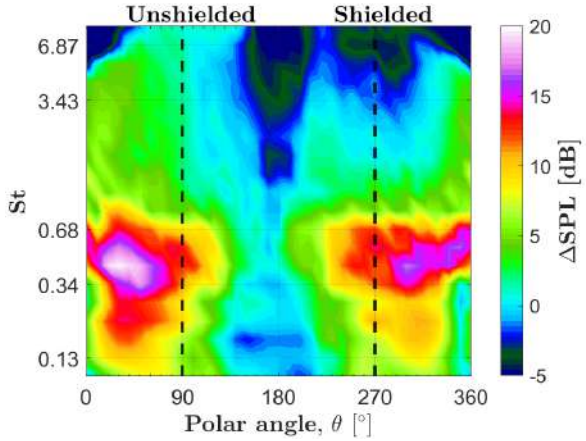

(c) ΔSPL (installation effects).

Figure 8: Contour of SPL in 1/3 octave bands showing both unshielded and shield sides.

6. CONCLUSIONS

A numerical study of the noise generated by isolated and installed jets was carried out through simulations based on the Lattice-Boltzmann Method for a Mach 0.7 cold jet. Far-field noise spectrum for both cases were obtained at θ=90° by using the Ffowcs-Williams and Hawkings analogy, which was verified through comparisons with experimental data. Maximum deviations of 2.3 dB for the isolated jet and around of 2.5 dB for the installed jet were observed. When analysed in terms of OASPL, the differences between numerical and experimental results were in the order of 0.5 dB. By analyzing the OASPL polar directivity pattern, maximum noise amplifications of 9.5 dB and 6.5 dB due to the installation effects were observed for θ<130° (unshielded side) and θ>210° (shielded side), respectively. The results obtained for the far-field spectrum showed that the additional noise due to the presence of the flapped plate occurs for St<0.68, reaching values up to 20 dB above the case considering an isolated jet. For this St range, the sound augmentation above the isolated jet case presented an asymmetric directivity pattern for the shielded and unshielded sides of the flapped plate, which is probably due to the inclination angle of the flap portion. The reflection and blockage effects for the installed jet showed to be significant at θ=90° and θ=270° for St>0.85, corresponding to the unshielded and shielded sides, respectively. These results confirmed that the installation effects depend on the St range.

7. ACKNOWLEDGEMENTS

This study was developed as part of a technical-scientific cooperation program between the Federal University of Santa Catarina and EMBRAER. The authors are also grateful to the Brazilian governmental agencies FINEP (agreement 0210/14) and CNPq (grant 465448/2014-3).

8. REFERENCES

Bastos, L.P., Deschamps, C.J., da Silva, A.R., Cordioli, J.A., Sirotto, J.R., Maia, I.A., Coelho, E.L. and Queiroz, R.L., 2018. "Development, validation and application of a newly developed rig facility for investigation of jet aeroacoustics". *Journal of the Brazilian Society of Mechanical Sciences and Engineering*, Vol. 40, No. 4, p. 171.

Bhatnagar, P.L., Gross, E.P. and Krook, M., 1954. "A model for collision processes in gases. i. small amplitude processes in charged and neutral one-component systems". *Physical review*, Vol. 94, No. 3, p. 511.

Brès, G., Nichols, J., Lele, S. and Ham, F., 2012. "Towards best practices for jet noise predictions with unstructured large eddy simulations". In *42nd AIAA Fluid Dynamics Conference and Exhibit*. p. 2965.

Brès, G., Pérot, F. and Freed, D., 2010. "A ffowcs williams-hawkings solver for lattice-boltzmann based computational aeroacoustics". In *16th AIAA/CEAS aeroacoustics conference*. Stockholm, Sweden, p. 3711.

Brown, C. and Bridges, J., 2006. "Small hot jet acoustic rig validation". *Technical Report NASA*.

Chapman, S., Cowling, T.G. and Burnett, D., 1990. *The mathematical theory of non-uniform gases: an account of the kinetic theory of viscosity, thermal conduction and diffusion in gases*. Cambridge Mathematical Library, Cambridge University Press.

Chen, H., Kandasamy, S., Orszag, S., Shock, R., Succi, S. and Yakhot, V., 2003. "Extended boltzmann kinetic equation for turbulent flows". *Science*, Vol. 301, No. 5633, pp. 633–636.

Chen, H. and Zhang, R., 2013. "Computer simulation of physical processes". US Patent App. 13/483,676.

Chen, H., Zhang, R. and Gopalakrishnan, P., 2017. "Lattice boltzmann collision operators enforcing isotropy and galilean invariance". US Patent 9,576,087.

Curle, N., 1955. "The influence of solid boundaries upon aerodynamic sound". *Proceedings of the Royal Society of London. Series A. Mathematical and Physical Sciences*, Vol. 231, No. 1187, pp. 505–514.

Da Silva, F.D., Deschamps, C.J., da Silva, A.R. and Simões, L.G., 2015. "Assessment of jet-plate interaction noise using the lattice boltzmann method". In *21st AIAA/CEAS Aeroacoustics Conference*. Dallas, TX, p. 2207.

Farassat, F. and Succi, G.P., 1982. "The prediction of helicopter rotor discrete frequency noise". In *In: American Helicopter Society, Annual Forum, 38th, Anaheim, CA, May 4-7, 1982, Proceedings.(A82-40505 20-01) Washington, DC, American Helicopter Society, 1982, p. 497-507.* pp. 497–507.

Ffowcs-Williams and Hall, L., 1970. "Aerodynamic sound generation by turbulent flow in the vicinity of a scattering half plane". *Journal of fluid mechanics*, Vol. 40, No. 4, pp. 657–670.

Guo, Z. and Shu, C., 2013. *Lattice Boltzmann method and its applications in engineering*, Vol. 3. World Scientific.

Head, R. and Fisher, M., 1976. "Jet/surface interaction noise-analysis of farfield low frequency augmentations of jet noise due to the presence of a solid shield". In *3rd Aeroacoustics Conference*. p. 502.

Hoheisel, H. and von Geyr, H.F., 2012. "The influence of engine thrust behaviour on the aerodynamics of engine airframe integration". *CEAS Aeronautical Journal*, Vol. 3, No. 1, pp. 79–92.

Jente, C., Pott-Pollenske, M., Boenke, D., Buescher, A. and Goldhahn, I., 2018. "Experimental investigation of jet-flap-interaction noise sensitivity due to varying flap parameters at a uhbr engine/high-lift-wing installation". In *2018 AIAA/CEAS Aeroacoustics Conference*. p. 3788.

Jordan, P., Jaunet, V., Towne, A., Cavalieri, A.V., Colonius, T., Schmidt, O. and Agarwal, A., 2018. "Jet–flap interaction tones". *Journal of Fluid Mechanics*, Vol. 853, pp. 333–358.

Kopiev, V.F., Belyaev, I.V., Faranosov, G.A., Kopiev, V., Ostrikov, N., Zaytsev, M.Y. and Paranin, G., 2014. "Numerical and experimental study of jfi effect on swept wing". In *20th AIAA/CEAS aeroacoustics conference*. p. 3060.

Launder, B.E. and Spalding, D.B., 1983. "The numerical computation of turbulent flows". In *Numerical prediction of flow, heat transfer, turbulence and combustion*, Elsevier, pp. 96–116.

Lawrence, J., 2014. *Aeroacoustic interactions of installed subsonic round jets*. Ph.D. thesis, University of Southampton.

Lawrence, J. and Self, R.H., 2015. "Installed jet-flap impingement tonal noise". In *21st AIAA/CEAS Aeroacoustics Conference*. p. 3118.

Lee, I., Zhang, Y. and Lin, D., 2019. "Experimental investigation of jet noise from a high bpr dual-stream jet in a static model-scale test". *Applied Acoustics*, Vol. 150, pp. 246–267.

Lew, P.T., Gopalakrishnan, P., Casalino, D., Shock, R., Li, Y., Zhang, R., Chen, H., Habibi, K. and Mongeau, L.G., 2014. "An extended lattice boltzmann methodology for high subsonic jet noise prediction". In *20th AIAA/CEAS Aeroacoustics Conference*. p. 2755.

Lyubimov, D., Maslov, V., Mironov, A., Secundov, A. and Zakharov, D., 2014. "Experimental and numerical investigation of jet flap interaction effects". *International Journal of Aeroacoustics*, Vol. 13, No. 3-4, pp. 275–302.

MacGregor, G., Ribner, H. and Lam, H., 1973. ""basic" jet noise patterns after deletion of convection and refraction effects: Experiments vs. theory". *Journal of Sound and Vibration*, Vol. 27, No. 4, pp. 437–454.

Mendez, S., Shoeybi, M., Lele, S. and Moin, P., 2013. "On the use of the ffowcs williams-hawkings equation to predict far-field jet noise from large-eddy simulations". *International Journal of Aeroacoustics*, Vol. 12, No. 1-2, pp. 1–20.

Mengle, V., 2011. "The effect of nozzle-to-wing gulley height on jet flow attachment to the wing and jet-flap interaction

noise". In *17th AIAA/CEAS Aeroacoustics Conference (32nd AIAA Aeroacoustics Conference)*. p. 2705.

Mockett, C., Fuchs, M., Kramer, F., Michel, U., Thiele, F. and Steger, M., 2017. "Further development and initial validation of innovative des-based approaches for the prediction of jet noise installation effects". In *ASME Turbo Expo 2017: Turbomachinery Technical Conference and Exposition*. American Society of Mechanical Engineers, pp. V02CT43A013–V02CT43A013.

Nogueira, P.A., Cavalieri, A.V. and Jordan, P., 2017. "A model problem for sound radiation by an installed jet". *Journal of Sound and Vibration*, Vol. 391, pp. 95–115.

Nogueira, P.A., Sirotto, J.R., Miotto, R.F., Cavalieri, A.V., Cordioli, J.A. and Wolf, W.R., 2019. "Acoustic radiation of subsonic jets in the vicinity of an inclined flat plate". *The Journal of the Acoustical Society of America*, Vol. 146, No. 1, pp. 50–59.

Rego, L.F., Avallone, F., Ragni, D., Casalino, D. and van der Velden, W.C., 2019. "Free-stream effects on jet-installation noise of a dual-stream engine". In *25th AIAA/CEAS Aeroacoustics Conference*. p. 2491.

Semiletov, V.A., Karabasov, S.A., Lyubimov, D.A., Faranosov, G.A. and Kopiev, V.F., 2013. "On the effect of flap deflection on jet flow for a jet-pylon-wing configuration: near-field and acoustic modelling results". In *19th AIAA/CEAS Aeroacoustics Conference*. p. 2215.

Shur, M.L., Spalart, P.R. and Strelets, M.K., 2005. "Noise prediction for increasingly complex jets. part i: Methods and tests". *International journal of aeroacoustics*, Vol. 4, No. 3, pp. 213–245.

Sirotto, J.R.d.L.N. *et al.*, 2016. "Validação experimental de bancada para medição de ruído de jatos". In *22th International Congress on Acoustics*. Buenos Aires, Argentina.

Teixeira, C.M., 1998. "Incorporating turbulence models into the lattice-boltzmann method". *International Journal of Modern Physics C*, Vol. 9, No. 08, pp. 1159–1175.

Tyacke, J.C., Wang, Z.N. and Tucker, P.G., 2019. "Les–rans of installed ultra-high-bypass-ratio coaxial jet aeroacoustics with flight stream". *AIAA Journal*, Vol. 57, No. 3, pp. 1215–1236.

van der Velden, W.C., Casalino, D., Gopalakrishnan, P., Jammalamadaka, A., Li, Y., Zhang, R. and Chen, H., 2018. "Jet noise prediction: Validation and physical insight". In *2018 AIAA/CEAS Aeroacoustics Conference*. p. 3617.

Witze, P.., 1974. "Centerline velocity decay of compressible free jets". *AIAA journal*, Vol. 12, No. 4, pp. 417–418.

9. RESPONSIBILITY NOTICE

The authors are the only responsible for the printed material included in this paper.